



## Biological cells and coupled electro-mechanical effects: The role of organelles, microtubules, and nonlocal contributions

Sundeep Singh <sup>a,\*</sup>, Jagdish A. Krishnaswamy <sup>a</sup>, Roderick Melnik <sup>a,b</sup>

<sup>a</sup> MS2Discovery Interdisciplinary Research Institute, Wilfrid Laurier University, 75 University Avenue West, Waterloo, Ontario, N2L 3C5, Canada

<sup>b</sup> BCAM - Basque Center for Applied Mathematics, Alameda de Mazarredo 14, E-48009, Bilbao, Spain

### ARTICLE INFO

**Keywords:**

Cell model  
Finite element modelling  
Electro-mechanical coupling  
Microtubules  
Medical therapies  
Piezoelectricity  
Flexoelectricity

### ABSTRACT

Biological cells are exposed to a variety of mechanical loads throughout their life cycles that eventually play an important role in a wide range of cellular processes. The understanding of cell mechanics under the application of external stimuli is important for capturing the nuances of physiological and pathological events. Such critical knowledge will play an increasingly vital role in modern medical therapies such as tissue engineering and regenerative medicine, as well as in the development of new remedial treatments. At present, it is well known that the biological molecules exhibit piezoelectric properties that are of great interest for medical applications ranging from sensing to surgery. In the current study, a coupled electro-mechanical model of a biological cell has been developed to better understand the complex behaviour of biological cells subjected to piezoelectric and flexoelectric properties of their constituent organelles under the application of external forces. Importantly, a more accurate modelling paradigm has been presented to capture the nonlocal flexoelectric effect in addition to the linear piezoelectric effect based on the finite element method. Major cellular organelles considered in the developed computational model of the biological cell are the nucleus, mitochondria, microtubules, cell membrane and cytoplasm. The effects of variations in the applied forces on the intrinsic piezoelectric and flexoelectric contributions to the electro-elastic response have been systematically investigated along with accounting for the variation in the coupling coefficients. In addition, the effect of mechanical degradation of the cytoskeleton on the electro-elastic response has also been quantified. The present studies suggest that flexoelectricity could be a dominant electro-elastic coupling phenomenon, exhibiting electric fields that are four orders of magnitude higher than those generated by piezoelectric effects alone. Further, the output of the coupled electro-mechanical model is significantly dependent on the variation of flexoelectric coefficients. We have found that the mechanical degradation of the cytoskeleton results in the enhancement of both the piezo and flexoelectric responses associated with electro-mechanical coupling. In general, our study provides a framework for more accurate quantification of the mechanical/electrical transduction within the biological cells that can be critical for capturing the complex mechanisms at cellular length scales.

### 1. Introduction

The mechanisms that affect the dynamics of the biological cell under the influence of extracellular mechanical stimulations have not been fully elucidated till date (Xue et al., 2015). The alterations of cell shape and structure during biomechanical interactions with the extracellular environments are not only critical to cellular processes such as growth, motility, differentiation, proliferation and apoptosis but also important for modern medical therapies such as tissue engineering and regenerative medicine (Basoli et al., 2018; Katti and Katti, 2017; McGarry and

Prendergast, 2004). Biological cells are constantly facing a variety of mechanical loading conditions that often result in changes in the cellular structure (Katti and Katti, 2017; Melnik et al., 2009). In light of this fact, there has been a growing interest in quantifying the mechanical properties of different elements of the cytoskeleton (Xue et al., 2015; Basoli et al., 2018; Katti and Katti, 2017; McGarry and Prendergast, 2004; Barreto et al., 2013). In particular, the cytoskeleton acts as a bridge between the intracellular and extracellular environments of the living cell and plays an important role in the cellular response to external stimuli (Katti and Katti, 2017; Barreto et al., 2013). Cytoskeleton

\* Corresponding author.

E-mail address: ssingh@wlu.ca (S. Singh).

comprises of different structural components, viz., microtubules, intermediate filaments and actin filaments. Several theoretical, computational and experimental studies have been reported in the quest for accurately quantifying the cellular response to mechanical stimuli (Basoli et al., 2018; Katti and Katti, 2017; McGarry and Prendergast, 2004; Barreto et al., 2013; Fallqvist et al., 2016; Jiang et al., 2017; Kononova et al., 2014; Ofek et al., 2009). Recent studies have also focused on dissecting the response of individual selected elements of cytoskeleton, for e.g., microtubules (tubular protein complexes composed of alpha and beta-tubulin monomers) owing to their important contribution to the elastic response of the cell along with their involvement in different key functions such as maintaining cell structure, intracellular transport and cell division (Havelka and Cifra, 2009; Li et al., 2017; Liew et al., 2015; Setayandeh and Lohrasebi, 2016; Thackston et al., 2019; Xiang and Liew, 2012).

Most of the previously reported computational studies for capturing the cell mechanics under external forces only consider the mechanical coupling between the applied stress and the induced strain. However, it has been widely reported that most of the biological molecules, such as microtubules, bones, collagen, etc., possess piezoelectric properties (Denning et al., 2017; Brown and Tuszyński, 1999; Chae et al., 2018; Chen-Glasser et al., 2018). It is noteworthy to mention that although piezoelectricity was discovered in 1880 by the Curie's, it was not formally studied and reported in the literature until the 1950s in biomaterials (Chae et al., 2018). Most of the pioneering work related to discovering piezoelectricity in the bone and wood was done by Fukada (Fukada, 1955; Fukada and Yasuda, 1957) and subsequently, several studies have been reported to quantify and investigate the piezoelectricity in other parts of the human body (Fukada, 1968, 1983, 2000; Fukada and Yasuda, 1964). The lack of inversion symmetry or non-centrosymmetric arrangement of dipole moments in most of the biological molecules (comprising of cellulose and various types of proteins, especially fibrous proteins) seems to be responsible for the induced piezoelectric characteristics in them (Chae et al., 2018; Chen-Glasser et al., 2018). In particular, piezoelectricity is an electro-mechanical effect induced due to linear coupling between the electric field and mechanical strain in the thermodynamic free energy description of the electro-elastic behavior of materials (Nguyen et al., 2013; Newnham, 2005). In addition, the two-way linear coupling of the piezoelectric biomaterials results in the conversion of mechanical deformation into an applied electric field and vice versa (Ahmadpoor and Sharma, 2015). Piezoelectricity is considered to be the dominant electro-mechanical transduction mechanism and has been widely used in different applications, including wearable sensors, flexible actuators, energy harvesting devices, advanced microscopes, artificial muscles and minimally invasive surgery (Ahmadpoor and Sharma, 2015; Labanca et al., 2008; Madden et al., 2004; Wang et al., 2010). It has been consistently considered as a fundamental property of biological tissues (Shamos and Levine, 1967), as well as other biological systems (Fukada, 1983; Anderson and Eriksson, 1970). Further, another electro-mechanical (nonlocal) effect that has received significantly less attention in this context is flexoelectricity, which is a consequence of the two-way linear coupling between the electric field and strain gradients as opposed to the coupling between the electric polarization and strain in piezoelectricity (Nguyen et al., 2013). Flexoelectricity is a size-dependent phenomenon that is induced due to the generated strain gradient that disrupts the inversion symmetry of the biomaterial due to the non-uniform displacement of atoms. Recently, flexoelectricity effects that originate from the polarization induced due to strain gradient have been observed in different types of biological samples, viz., lipid bilayer, hair cell, viruses, etc. (Nguyen et al., 2013). It is noteworthy to mention that piezoelectricity is produced by uniform strains while flexoelectricity appears from inhomogeneous strains or a strain gradient. From the theoretical perspective, linear piezoelectricity is a coupling between a single strain component and a single electric field component and occurs only in non-centrosymmetric materials such as BaTiO<sub>3</sub>. However,

flexoelectricity is a coupling between a strain-gradient component and an electric field component. This can occur even in centrosymmetric materials and the effect is especially magnified in the presence of inhomogeneities at small length scales, which can give rise to large strain gradients and consequent flexoelectric generation of electric fields/-fluxes. Thus, relative to piezoelectric effects the flexoelectric effects are insignificant at the macroscopic scale but become predominant at mesoscopic or smaller length scales (Nguyen et al., 2013), where strain gradients become considerably large. In the context of the biological cell, the nanoscale cross-sections of rigid microtubules in a soft cellular matrix can produce significant strain-gradients. Therefore, we anticipate flexoelectric contributions to electro-mechanical coupling, in this case, to be non-trivial.

In what follows, the present study includes the effects of piezoelectricity and flexoelectricity while modelling cell mechanics under the influence of external mechanical loads. A finite element model of the single biological cell has been developed using continuum modelling of critically important organelles, viz., nucleus, mitochondria, microtubules, cell membrane and cytoplasm. The overall objective of this study is to examine the influence of applied forces from the extracellular side on the single-cell mechanics. A fully-coupled electro-mechanical model of a biological cell has been developed to quantify the effect of induced strains and strain gradient on the electric potential generation by considering linear piezoelectric effects and nonlocal effects such as flexoelectricity. In what follows, we demonstrate that the effect of flexoelectricity is more pronounced as compared to piezoelectricity in the biological cells at smaller length scales.

## 2. Materials and methods

This section provides the details of the computational model of the biological cell along with the considered material properties (section 2.1), mathematical framework of the coupled electro-mechanical model (section 2.2), as well as the numerical setup and necessary boundary conditions used to solve the proposed problem (section 2.3).

### 2.1. Computational domain of the biological cell

The computational domain with different organelles considered in the present study has been derived from previous studies such as (Barreto et al., 2013; Ofek et al., 2009; Barvitenko et al., 2018; Bhowmik and Pilon, 2016; Li et al., 2015) and has been presented in Fig. 1. A 20 μm diameter cell has been embedded with a nucleus (5 μm diameter), mitochondria (0.92 μm diameter) and microtubules (25 nm diameter).

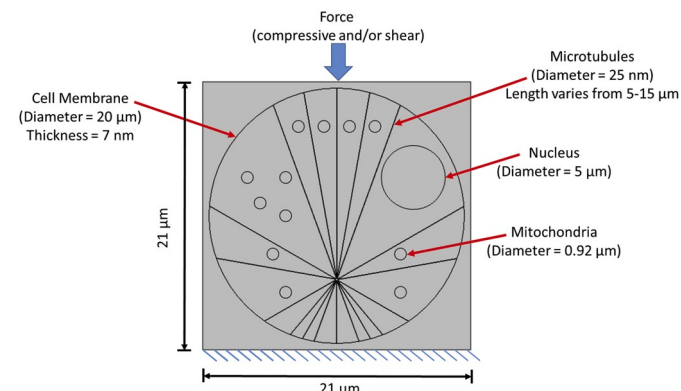


**Fig. 1.** Schematic of the two-dimensional model of biological cell considering various organelles, viz., cell membrane (20 μm in diameter), nucleus (5 μm in diameter), mitochondria (0.92 μm in diameter) and microtubules (25 nm in diameter). The external force is applied at the top surface of the cell, while the bottom surface of the cell is subjected to fixed and electrically grounded boundary conditions.

Importantly, the arrangement of varying lengths of microtubules connected at the centrosome has been derived from (Barreto et al., 2013; Ofek et al., 2009; Barvitenko et al., 2018). The cell membrane has been modelled to separate the cytoplasmic (interior) side of the cell with the extracellular matrix (external) side. The material properties considered in the present study for different cell organelles have been presented in Table 1 (Katti and Katti, 2017; Denning et al., 2017; Li et al., 2015; Gowrishankar et al., 2006; Tiwari et al., 2009; Kalra et al., 2019). Notably, it has been widely reported that microtubules possess piezoelectricity (Brown and Tuszyński, 1999), thus the present study considers the piezoelectric and flexoelectric coefficients only for microtubules and for the rest of the organelles these coefficients have been considered to be zero.

## 2.2. Coupled electro-mechanical model of biological cell

The fully coupled electro-mechanical model for the two-dimensional biological cell domain in a steady-state regime has been derived from the extended linear theory of continuum mechanics for dielectric continua, in which the strain gradient is incorporated (Krishnaswamy, 2019a, 2019b, 2019c). The developed model will consider the effects of linear piezoelectricity in addition to the strain gradient electricity or flexoelectricity. The electric Gibbs free energy function derived from the thermodynamical framework that includes the couplings between strain, strain gradients and electric fields is given by (Abdollahi et al., 2014; Bahrami-Samani et al., 2010; He et al., 2019; Gizzi et al., 2015; Pandolfi et al., 2016)

$$G = \frac{1}{2}c_{ijkl}\epsilon_{ij}\epsilon_{kl} - \frac{1}{2}\kappa_{ij}E_iE_j - e_{kij}E_k\epsilon_{ij} - \mu_{ijkl}E_i\epsilon_{jk,l}, \quad (1)$$

**Table 1**  
Electro-mechanical characteristics of different biomaterials used in the present study.

Parameter	Value	References
<b>Elastic coefficients</b>		
Elastic modulus of microtubules	1.9 GPa	Katti and Katti (2017)
Poisson's ratio of microtubules	0.3	Katti and Katti (2017)
Elastic modulus of cytoplasm and extracellular matrix	0.25 kPa	Katti and Katti (2017)
Poisson's ratio of cytoplasm and extracellular matrix	0.49	Katti and Katti (2017)
Elastic modulus of nucleus	1 kPa	Katti and Katti (2017)
Poisson's ratio of nucleus	0.3	Katti and Katti (2017)
Elastic modulus of mitochondria	50.3 kPa	Li et al. (2015)
Poisson's ratio of mitochondria	0.3	Assumed
Elastic modulus of cell membrane	1.8 kPa	Katti and Katti (2017)
Poisson's ratio of cell membrane	0.3	Katti and Katti (2017)
<b>Relative permittivity</b>		
Microtubules	40	Kalra et al. (2019)
Cytoplasm and extracellular matrix	80	(Gowrishankar et al., 2006; Tiwari et al., 2009)
Nucleus	80	(Gowrishankar et al., 2006; Tiwari et al., 2009)
Mitochondria	80	(Gowrishankar et al., 2006; Tiwari et al., 2009)
Cell Membrane	3	(Gowrishankar et al., 2006; Tiwari et al., 2009)
<b>Piezoelectric coefficients</b>		
$d_{14}$	-12 pC/ N	Denning et al. (2017)
$d_{15}$	6.21 pC/ N	Denning et al. (2017)
$d_{31}$	-4.84 pC/N	Denning et al. (2017)
$d_{33}$	0.89 pC/ N	Denning et al. (2017)
<b>Flexoelectric coefficients</b>		
Longitudinal, $\mu_{11}$	1 nC/m	Assumed
Transverse, $\mu_{12}$	1 nC/m	
Shear, $\mu_{44}$	0	

where  $c_{ijkl}$  is the fourth-order tensor of elastic moduli,  $\epsilon_{ij}$  is the second-order mechanical strain tensor,  $\kappa_{ij}$  is the second-order dielectric tensor,  $e_{ijk}$  is the third-order piezoelectric tensor,  $E_l$  is the electric field vector,  $\mu_{ijkl}$  is the fourth-order flexoelectric tensor and  $\epsilon_{jk,l}$  is the strain gradient. The typical linear piezoelectric models discussed widely in the literature would have only the first three terms on the right-hand side, thus clearly overlooking the nonlocal effects (Chae et al., 2018; Krishnaswamy et al., 2019b, Krishnaswamy, 2019c).

The phenomenological relations describing the coupling of the mechanical and electrical fields in linear, homogeneous and isotropic elastic dielectric materials derived from Eq. (1) under an infinitesimal deformation are expressed as follows

$$\sigma_{ij} = \frac{\partial G}{\partial \epsilon_{ij}} = c_{ijkl}\epsilon_{kl} - e_{kij}E_k, \quad (2)$$

$$\hat{\sigma}_{ijk} = \frac{\partial G}{\partial \epsilon_{ijk}} = \mu_{ijk}E_l, \quad (3)$$

$$D_i = -\frac{\partial G}{\partial E_i} = \kappa_{ij}E_j + e_{ijk}\epsilon_{jk} + \mu_{ijkl}\epsilon_{jk,l}, \quad (4)$$

where  $\sigma_{ij}$  is the classical second-order Cauchy stress tensor,  $\hat{\sigma}_{ijk}$  is the higher-order stress tensor arising from flexoelectricity,  $D_i$  is the electric displacement vector,  $\frac{\partial G}{\partial \epsilon_{ij}}$  is the partial derivative of Gibbs free energy with respect to strain,  $\frac{\partial G}{\partial \epsilon_{ijk}}$  is the partial derivative of Gibbs free energy with respect to strain gradient,  $\frac{\partial G}{\partial E_i}$  is the partial derivative of Gibbs free energy with respect to electric field and subscript represents the components of the vector or tensor quantities that range from 1 to 3. More details about the reduction of Gibbs free energy equation (Eq. (1)) to the above form of equations (Eqs. (2)–(4)) along with a detailed description of transformation, symmetry, matrices, tensor properties and notations can be found in (Newnham, 2005; Parton and Kudryavtsev, 1988; Uchino, 2009). The relationship between the strain ( $\epsilon_{ij}$ ) and displacement ( $u_i$ ), and electric field ( $E_i$ ) and electric potential ( $\phi$ ) is given by Eq. (5) and Eq. (6), respectively

$$\epsilon_{ij} = \frac{1}{2}(u_{i,j} + u_{j,i}), \quad (5)$$

$$E_i = -\phi_i. \quad (6)$$

The constitutive relations described above are further subjected to conditions of equilibrium and Gauss's law with the assumption of vanishing body forces and vanishing volume charge density and is given by (Mao and Purohit, 2014; Sharma et al., 2010)

$$(\sigma_{ij} - \hat{\sigma}_{ijk,k})_j + F_i = 0, \quad (7)$$

$$D_{i,i} = 0, \quad (8)$$

where  $F_i$  represent the components of the body forces.

Since collagen and microtubule-associated tau protein shares the same crystalline homology (de Garcini et al., 1990), thus motivated by (Kushagra, 2015) it has been assumed that the piezoelectric potential generation in the two proteins under the application of similar forces would be analogous. Therefore, in the present study, the piezoelectric coefficients of microtubules have been considered similar to that of collagen and have been adapted from (Denning et al., 2017). Assuming hexagonal symmetry, the piezoelectric coefficients in the strain-charge form and using Voigt notation are given as (Denning et al., 2017)

$$d_{ij} = \begin{bmatrix} 0 & 0 & 0 & d_{14} & d_{15} & 0 \\ 0 & 0 & 0 & d_{15} & -d_{14} & 0 \\ d_{31} & d_{31} & d_{33} & 0 & 0 & 0 \end{bmatrix}, \quad (9)$$

where the subscript  $i$  of the piezoelectric tensor represents the direction

of electric field displacement and the subscript  $j$  represents the associated mechanical deformation.

Since the present study is formulated using the stress form, thus the piezoelectric coefficients in strain form given in Eq. (9) have been converted into the stress form utilizing the following relation

$$e_{ijk} = c_{jklm} d_{ilm}, \quad (10)$$

where  $e_{ijk}$  are the piezoelectric stress coefficients,  $c_{jklm}$  are the components of the elastic tensor and  $d_{ilm}$  are the piezoelectric strain coefficients given in Eq. (9).

Further, the effects of orientation on the piezoelectric tensor of microtubules have also been accounted for in the present study. The transformation of the piezoelectric coefficients from the old coordinate system (e.g.,  $x$ ,  $y$  and  $z$ ) to the new coordinate system (e.g.,  $x'$ ,  $y'$  and  $z'$ ) is given by (Kiran et al., 2018)

$$\dot{e}_{ijk} = ae_{ijk}\alpha, \quad (11)$$

where  $a$  is the matrix of rotation about any transformed axis, given by Eq. (12) and  $\alpha$  is the matrix obtained from the direction cosines of old coordinate system transformed into the new coordinate system and is given by Eq. (13). Specifically, we have:

$$a = \begin{bmatrix} l_1^2 & m_1^2 & n_1^2 \\ l_2^2 & m_2^2 & n_2^2 \\ l_3^2 & m_3^2 & n_3^2 \end{bmatrix}, \quad (12)$$

$$\alpha = \begin{bmatrix} l_1^2 & m_1^2 & n_1^2 & 2m_1n_1 & 2n_1l_1 & 2l_1m_1 \\ l_2^2 & m_2^2 & n_2^2 & 2m_2n_2 & 2n_2l_2 & 2l_2m_2 \\ l_3^2 & m_3^2 & n_3^2 & 2m_3n_3 & 2n_3l_3 & 2l_3m_3 \\ l_2l_3 & m_2m_3 & n_2n_3 & m_2n_3 + n_2m_3 & l_2n_3 + n_2l_3 & m_2l_3 + l_2m_3 \\ l_3l_1 & m_3m_1 & n_3n_1 & m_1n_3 + n_1m_3 & l_1n_3 + n_1l_3 & m_1l_3 + l_1m_3 \\ l_1l_2 & m_1m_2 & n_1n_2 & m_1n_2 + n_1m_2 & l_1n_2 + n_1l_2 & m_1l_2 + l_1m_2 \end{bmatrix} \quad (13)$$

$$\begin{aligned} l_1 &= \cos(x', x) & m_1 &= \cos(y', x) & n_1 &= \cos(z', x) \\ \text{where } l_2 &= \cos(x', y) & m_2 &= \cos(y', y) & n_2 &= \cos(z', y) \\ l_3 &= \cos(x', z) & m_3 &= \cos(y', z) & n_3 &= \cos(z', z) \end{aligned}$$

Considering the two-dimensional model of the biological cell described in section 2.1 and assuming transversely isotropic piezoelectric material along the  $x_3$ -axis, the  $x_1 - x_3$  or  $x_2 - x_3$  plane is isotropic and either of these could be employed for studying the plane electro-mechanical phenomena. Therefore, assuming the  $x_1 - x_3$  plane (i.e.  $\varepsilon_{22} = \varepsilon_{12} = \varepsilon_{23} = 0$ ,  $E_2 = 0$ ), the phenomenological equations (Eqs. (2)–(4)) using Voigt notation are reduced to the matrix form as follows (Krishnaswamy et al., 2019a, 2019b, 2019c; Saputra et al., 2018)

$$\begin{bmatrix} \sigma_{11} \\ \sigma_{33} \\ \sigma_{13} \end{bmatrix} = \begin{bmatrix} c_{11} & c_{13} & 0 \\ c_{13} & c_{33} & 0 \\ 0 & 0 & c_{44} \end{bmatrix} \begin{bmatrix} \varepsilon_{11} \\ \varepsilon_{33} \\ 2\varepsilon_{13} \end{bmatrix} - \begin{bmatrix} 0 & e_{31} \\ 0 & e_{33} \\ e_{15} & 0 \end{bmatrix} \begin{bmatrix} E_1 \\ E_3 \end{bmatrix}, \quad (14)$$

$$\begin{bmatrix} D_1 \\ D_3 \end{bmatrix} = \begin{bmatrix} 0 & 0 & e_{15} \\ e_{31} & e_{33} & 0 \end{bmatrix} \begin{bmatrix} \varepsilon_{11} \\ \varepsilon_{33} \\ 2\varepsilon_{13} \end{bmatrix} + \begin{bmatrix} \kappa_{11} & 0 \\ 0 & \kappa_{33} \end{bmatrix} \begin{bmatrix} E_1 \\ E_3 \end{bmatrix} + \begin{bmatrix} \mu_{1111} & \mu_{1331} \\ \mu_{3113} & \mu_{3333} \end{bmatrix} \begin{bmatrix} \varepsilon_{11,1} & \varepsilon_{33,1} \\ \varepsilon_{11,3} & \varepsilon_{33,3} \end{bmatrix}, \quad (15)$$

where  $c_{11} = \lambda_m + 2\mu_m$ ,  $c_{13} = \lambda_m$ ,  $c_{33} = \lambda_m + 2\mu_m$  and  $c_{44} = \mu_m$ . The terms  $\lambda_m$  and  $\mu_m$  are the Lame's constants and are given by  $\lambda_m = \frac{E_m \nu_m}{(1+\nu_m)(1-2\nu_m)}$  and  $\mu_m = \frac{E_m}{2(1+\nu_m)}$ , where  $E_m$  is the elastic modulus and  $\nu_m$  is the Poisson's ratio presented in Table 1 for different organelles of the biological cell. Further, the non-zero higher-order stresses arising from flexoelectricity in the two-dimensional model of the biological cell are given by

$$\hat{\sigma}_{111} = \mu_{1111} E_1, \quad (16)$$

$$\hat{\sigma}_{113} = \mu_{3113} E_3, \quad (17)$$

$$\hat{\sigma}_{331} = \mu_{1331} E_1, \quad (18)$$

$$\hat{\sigma}_{333} = \mu_{3333} E_3, \quad (19)$$

where  $\mu_{1111} = \mu_{3333} = \mu_{11}$  is the longitudinal flexoelectric coefficient and  $\mu_{1331} = \mu_{3113} = \mu_{13}$  is the shear flexoelectric coefficient as presented in Table 1.

### 2.3. Numerical implementation

In this section, a fully coupled electro-mechanical model derived in section 2.2 has been numerically implemented to quantify the role of linear piezoelectric and nonlocal effects under the application of external mechanical stimuli. The bottom surface of the two-dimensional model of biological cell presented in Fig. 1 has been subjected to fixed and electrically grounded boundary conditions. In particular, the fixed boundary condition at the bottom has been adopted from previous studies (Garcia and Garcia, 2018a, 2018b; Li et al., 2018; Marcotti et al., 2019), whereby the cell is placed on the rigid support and the force is applied at the top to quantify the mechanical response of the single cell. Since the biological cell is exposed to a variety of forces from the extracellular side, in order to better understand the mechanics of cells, different magnitudes and directions of the applied forces have also been considered in this study. The range of forces considered in the present study varies from 0.02 nN to 0.1 nN and has been adopted from (Katti and Katti, 2017). Importantly, a constant displacement (representing either compressive and/or shear force) boundary condition has been applied at the top surface of the cell with different magnitudes (20 nm, 60 nm and 120 nm) (Katti and Katti, 2017) and the induced stresses, strains, electric field and electric potential have been computed. In our analysis, the strain gradients were not directly specified at the boundary, rather displacement boundary conditions were prescribed from which the strain gradients were determined from the FEM solution. Thus, the flexoelectricity has been computed only by considering the electro-mechanical variations occurring within the biological cell that has been modelled as a composite comprising of different organelles. The quantification of flexoelectricity generated due to a deliberate external application of a strain gradient requires further modification of the boundary conditions for introducing higher-order functions of the boundary displacements, which has not been considered in the present analysis (Krishnaswamy et al., 2020). The coupled electro-mechanical models of biological cells subjected to external stimuli have been solved using a finite-element method (FEM) based commercial COMSOL Multiphysics 5.2 software (COMSOL AB, Stockholm, Sweden). A standard Lagrange (quadratic) shape function has been used in our FEM analysis to discretize the space domain for the physical field. The governing equations of the fully-coupled electro-mechanical models were solved adopting a multifrontal massively parallel sparse (MUMPS) direct solver with a default preordering algorithm. The numerical convergence was attained below the pre-specified value (i.e.  $10^{-5}$ ) of the relative tolerance for all simulations. The computational domain has been discretized using an optimal number of heterogeneous triangular mesh elements (obtained after conducting a mesh convergence analysis) using COMSOL's built-in mesh generator. Fig. 2(a) presents the meshed computational domain of biological cell comprising of 298052 elements and 1788531 degrees of freedom. The result of the grid independence analysis with different mesh element sizes considering a coupled electro-mechanical model of a biological cell with both piezo and flexoelectric effects has been presented in Fig. 2(b). The maximum electric field intensity (in log(V/m)) computed from the model along with the increase in computational cost relative to minimum element

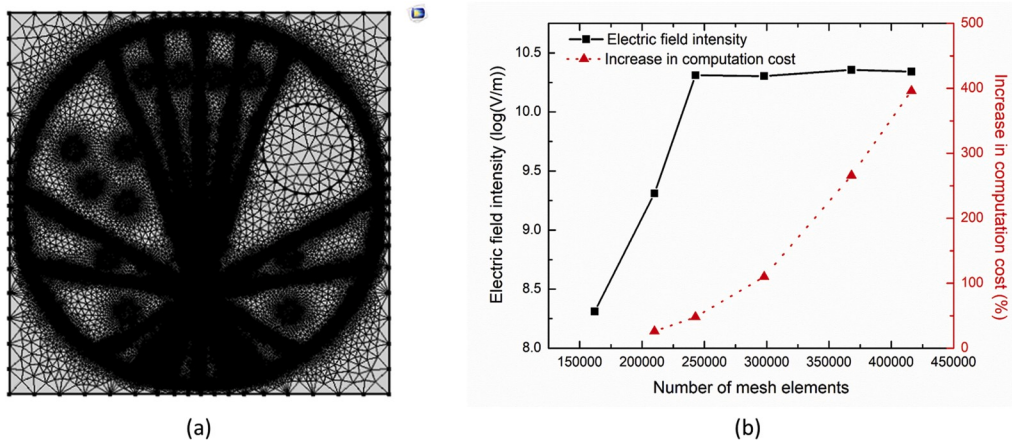


**Fig. 2.** (a) Meshed computational domain of biological cell comprising of 298052 heterogeneous triangular elements, and (b) results of grid independence study.

size has been shown in Fig. 2(b). Importantly, a trade-off between the mesh element size and computational cost has been used for saving time and memory requirements and accordingly the mesh with 298052 elements has been selected in the present analysis. All simulations have been conducted on a Dell T7400 workstation with Quad-core 2.0 GHz Intel® Xeon® processors.

### 3. Results and discussion

In the present numerical study, a coupled electro-mechanical model of the biological cell has been developed using FEM. The main novelty of

the present work is to quantify the electric potential generation and electric field distribution considering both piezoelectric and flexoelectric effects within the biological cell (as presented in Fig. 1) under the influence of various forces applied from the extracellular side. The biological cell is approximated as a composite comprising of the different organelles (viz., microtubules, mitochondria and cell nucleus) placed randomly within the two-dimensional domain. In this section, we present a comparative analysis of the consideration of piezoelectric effect with and without the inclusion of flexoelectric effects within the cellular system. The associated limitations of the present model along with possible future extensions have also been highlighted.

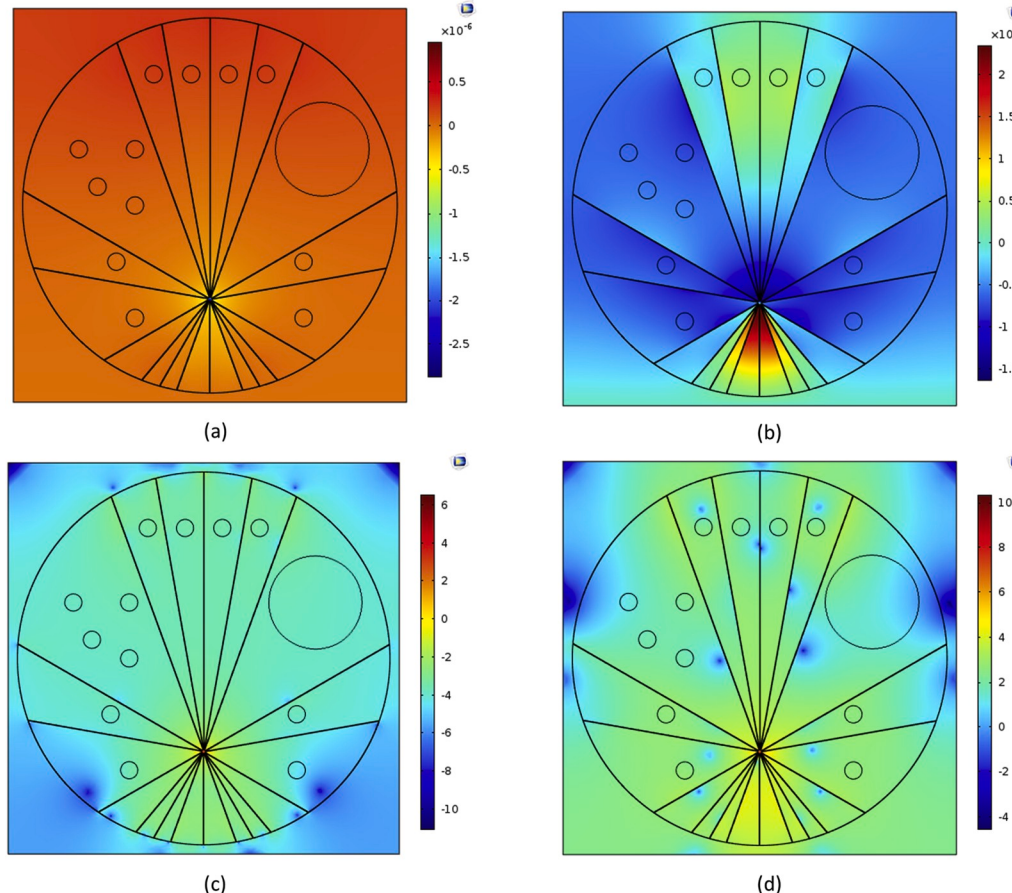


**Fig. 3.** The electric potential (in V) (a-b) and electric field distribution (in  $\log(V/m)$ ) (c-d) predicted with the compressive displacement of 60 nm at the top surface of the cell with: (a, c) piezoelectric coupling and (b, d) both piezo and flexoelectric couplings.

### 3.1. Comparative analysis of the piezoelectric and flexoelectric contributions to the electro-elastic response

The electric potential distribution, obtained within the biological cell under the influence of 60 nm compressive displacement applied at the top surface, has been presented in Fig. 3(a)-(b). Importantly, Fig. 3(a) gives the electric potential distribution considering only the piezoelectric effect while Fig. 3(b) gives the electric potential distribution considering both the piezoelectric and flexoelectric effects. As evident from Figs. 3(a)-(b), there prevails significant variations in the electric potential distribution obtained utilizing the effects of linear piezoelectric and nonlocal flexoelectric contributions. The electric potential generated within the biological cell considering both the piezoelectric and flexoelectric effects results in almost two orders of magnitude higher as compared to the case when only the piezoelectric effect is considered. Further, the maximum magnitude of the electric potential is generated in the region just beneath the centrosome (where microtubules are connected). This can be attributed to the higher values of the strains and strain-gradients that will be presented in the subsequent section. The electric field intensity distribution obtained with consideration of piezoelectric effect alone and considering both piezoelectric and flexoelectric effects have been presented in Fig. 3(c) and (d), respectively. It can be clearly seen that the maximum value of electric field intensity is localized at the edges of microtubules in both cases which is in agreement with the results reported in previous studies (e.g., (Havelka et al., 2011; Kučera and Havelka, 2012)). Again, the maximum electric field intensity obtained with considering both the piezoelectric and flexoelectric effects is 4 orders of magnitude higher as compared to when the piezoelectric contribution was considered alone. Thus, the obtained results clearly demonstrate the importance of consideration of both piezoelectric and flexoelectric effects on the electro-elastic response of biological cells that becomes predominant at smaller length scales. Furthermore, the parametric analysis for different numbers of microtubules within the two-dimensional cellular domain has also been carried out to quantify the electro-elastic response under the application of 60 nm compressive displacement at the top surface and fixed bottom. The electric potential and electric field distribution for different

numbers of microtubules (viz., 2, 6, 10, 14 and 18) considering both piezo and flexoelectric couplings are presented in Figs. 4 and 5, respectively. As evident from Figs. 4 and 5, the maximum value of electric potential and electric field intensity increases with the increase in the number of microtubules from 2 to 18. The visual representation of electric potential and electric field distribution presented in Figs. 4 and 5 are useful in highlighting the areas where such parameters are localized. Furthermore, the specific quantification of the electro-mechanical effects of microtubules under different loading configurations has also been presented in Fig. 6. It can be seen from Fig. 6(a) that the deviation among the maximum generated electric potentials due to the electro-mechanical coupling within the biological cell increases as the applied compressive displacement at the top surface of the cell increases from 20 nm to 120 nm. Thus, the number of microtubules and loading conditions significantly influence the electro-elastic response of the two-dimensional biological cell considered in the present study. It is noteworthy to mention that a biological cell would typically have more than 18 microtubules (the maximum number considered in our developed model) and therefore we expect a significant enhancement in the magnitude of the electro-mechanical effects as reported in this study. This enhanced coupling would be quite useful in a number of important applications in the field of biocompatible nano-biosensors, drug delivery, noninvasive diagnostic techniques and treatment approaches (Chae et al., 2018).

### 3.2. Effect of variations in the applied forces on the piezoelectric and flexoelectric contributions to the electro-elastic response

As mentioned earlier, in the present two-dimensional model of an idealized cell a displacement boundary condition is used at the top surface of the cell while the bottom surface is fixed. Accordingly, the magnitude of the displacements considered in the present numerical study has been considered to be 20 nm, 60 nm and 120 nm (Katti and Katti, 2017). The effect of the different magnitude of the applied compressive displacements at the top surface of the biological cell on the electric potential and electric field distributions has been presented in Fig. 7. As evident from Figs. 7(a)-(c), the maximum electric potential

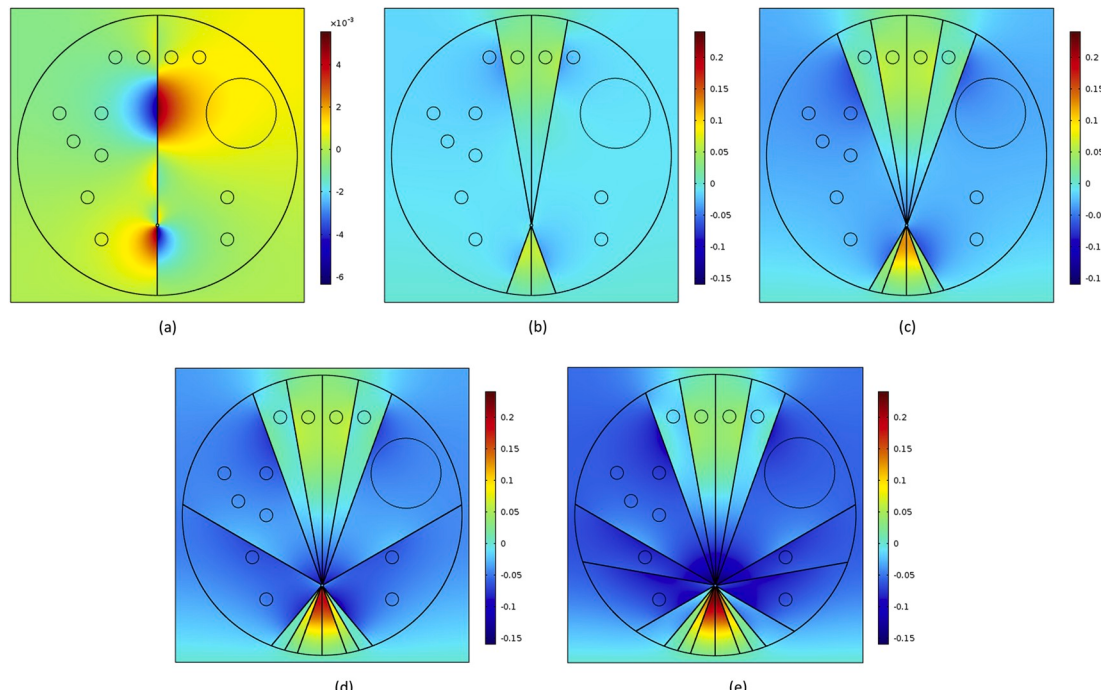


**Fig. 4.** The electric potential distribution (in mV) predicted with both piezo and flexoelectric couplings under the compressive displacement of 60 nm at the top surface of the biological cell with (a) 2, (b) 6, (c) 10, (d) 14 and (e) 18 microtubules.

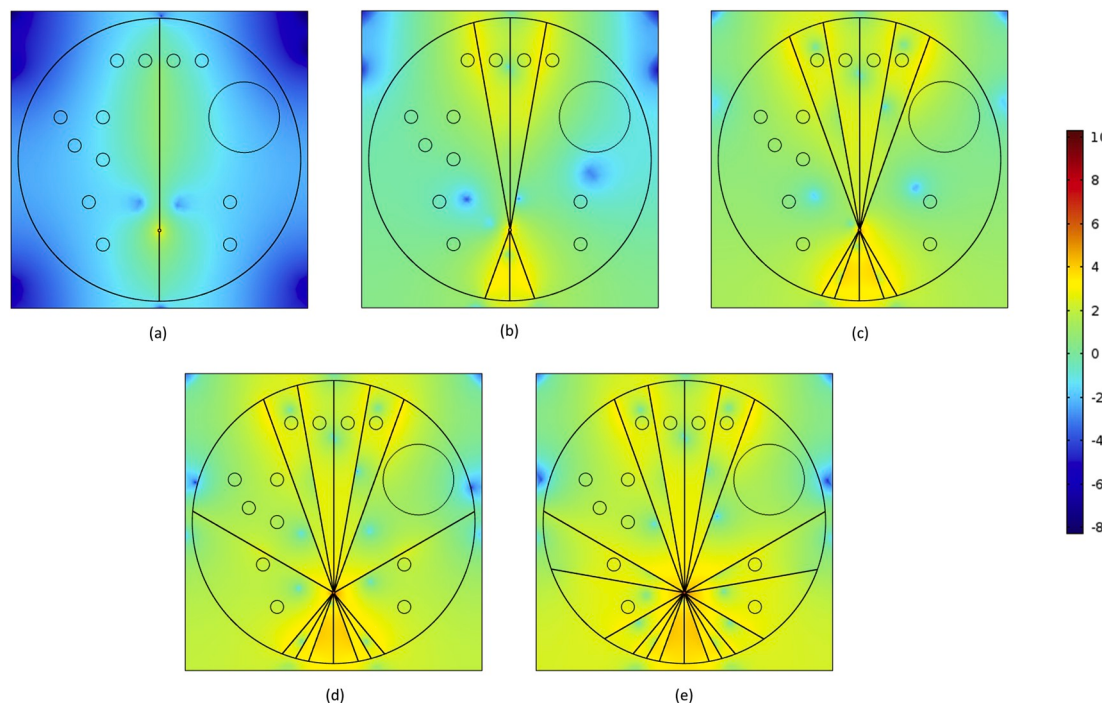


**Fig. 5.** The electric field distribution (in  $\log(\text{V/m})$ ) predicted with both piezo and flexoelectric couplings under the compressive displacement of 60 nm at the top surface of the biological cell with (a) 2, (b) 6, (c) 10, (d) 14 and (e) 18 microtubules.

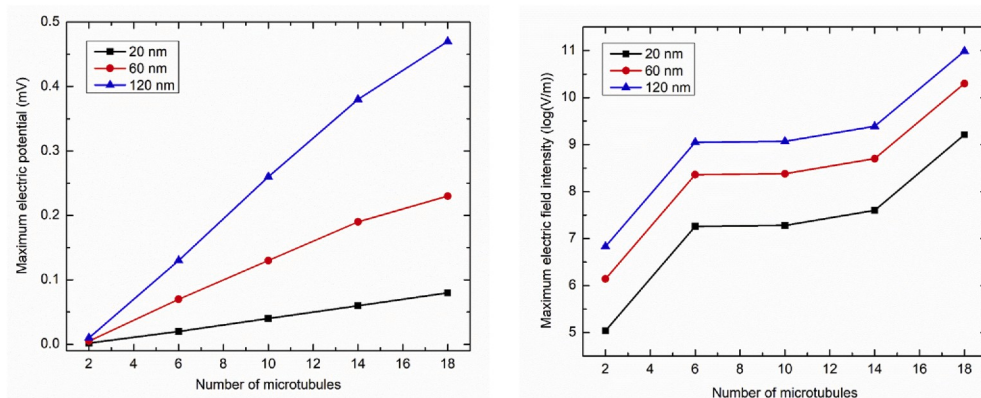


**Fig. 6.** Variation of the maximum of: (a) electric potential and (b) electric field intensity, predicted with both piezo and flexoelectric couplings under the compressive displacement of 20 nm, 60 nm and 120 nm at the top surface of the biological cell with different numbers of microtubules.

obtained considering only the piezoelectric effect in the coupled electro-mechanical model increases with the increase of applied load. It has been found that the increase of the compressive displacement from 20 nm to 120 nm increases the maximum generated potential from 0.0002 mV to 0.001 mV. Similar trends have been obtained when the flexoelectric effect is introduced within the coupled model (Figs. 7 (d)-(f)), although the magnitude of the electric potential generated is far higher among all cases as compared to considering piezoelectric effect alone. The maximum electric potential for the compressive displacements of 20 nm, 60 nm and 120 nm considering both piezoelectric and flexoelectric effects has been predicted to be 0.06 mV, 0.2 mV and 0.4 mV, respectively.

Apart from the variation of the magnitude of the force, the effect of variation in the direction of applied force/displacement has also been analyzed in the present study. Three different cases have been considered, viz., application of 60 nm: (a) compressive displacement, (b) shear displacement, and (c) both shear and compressive displacements. The maximum electric potential and electric field intensity obtained for

different considered cases have been summarized in Table 2. The application of compressive displacement (i.e. in x-axis) results in higher electric potential and electric field generation for both piezoelectric as well as combined (piezoelectric and flexoelectric) effects as compared to when the shear displacement (i.e. in y-axis) is applied. Further, the application of 60 nm displacement in both compressive and shear directions results in the maximum electric potential generation of 0.0038 mV considering the piezoelectric effect alone and 0.29 mV considering both piezoelectric and flexoelectric effects. However, the maximum magnitude of the electric field intensity for combined compressive and shear displacements has been found to be similar to the case when compressive displacement was applied alone.

The quantitative comparisons of the electro-elastic response of the coupled electro-mechanical model of a biological cell with and without flexoelectric coupling have been presented in Fig. 8. The predicted outcomes of the model, viz., electric potential and electric field intensity have been presented across the two selected lines within the two-dimensional domain of the biological cell, as shown in Fig. 8(a). Both

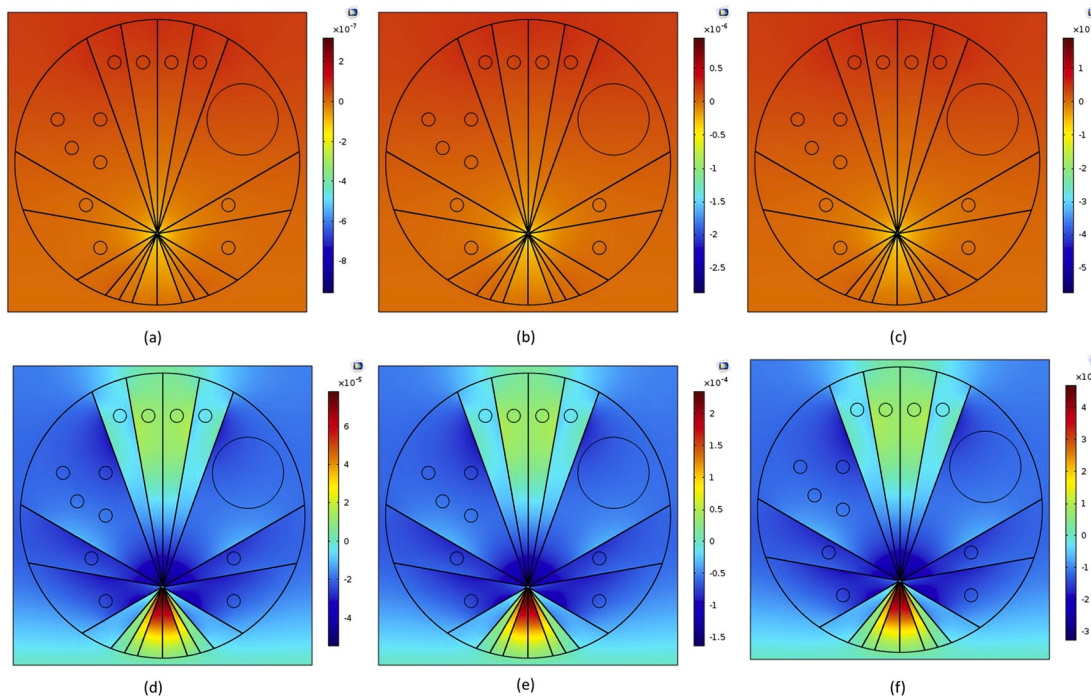


**Fig. 7.** The electric potential distribution (in V) predicted with (a-c) piezoelectric coupling and (d-f) both piezo and flexoelectric couplings under the compressive displacement of: (a, d) 20 nm, (b, e) 60 nm, and (c, f) 120 nm at the top surface of the biological cell.

**Table 2**

Comparision of maximum electric potential and electric field intensity attained with the piezoelectric and flexoelectric model under the application of initial displacement of 60 nm in different directions.

Applied displacement (nm)	Maximum electric potential (mV)		Maximum magnitude of electric field (log(V/m))		
	x-axis	y-axis	Piezo	Flexo	
0	-60	$2.88 \times 10^{-3}$	0.23	6.50	10.30
60	0	$0.25 \times 10^{-3}$	0.045	3.94	7.16
60	-60	$3.83 \times 10^{-3}$	0.29	6.85	10.69

the considered horizontal and vertical lines pass from the center of the centrosome where microtubules are connected. The electric potential generated under the application of 60 nm displacement at the top surface of the cell with a fixed and grounded bottom has been presented in Figs. 8(b-g) for different loading conditions considered in the present study, i.e. compressive, shear and combined (both compressive and shear). As evident from Figs. 8(b-g), significant variation prevails among the predicted values of the electric potential across both the horizontal (Figs. 8(b-d)) and vertical lines (Figs. 8(e-g)). For all the cases, the electric potential generated with both piezo and flexoelectric coupling is on a higher side as compared to the piezoelectric coupling alone. Further, among all cases, the maximum variation is induced at the centrosome region where the microtubules are connected. Similar trends have been obtained for the electric field intensity as presented in Figs. 8(h-m).

The total displacement distribution for different directions of 60 nm applied displacements, viz., compressive, shear and compressive plus shear has been presented in Fig. 9. As evident from Fig. 9, the maximum deformation is induced near the top surface of the biological cells where the displacement was applied in the coupled electro-mechanical model. The bottom surface of the biological cell experiences zero deformation due to fixed boundary conditions applied at that surface. When the compressive load is applied, the deformation pattern is highly non-uniform typically at the microtubules ends just lying beneath the top surface, clearly highlighting one of the main purposes of the

microtubules, i.e. to maintain the cellular rigidity under the action of external forces. Further, the application of shear load leads to low deformations at the microtubules just lying beneath the top surface as compared to that obtained with the compressive load. Moreover, the distribution of induced strain gradients  $\epsilon_{11,1}$  and  $\epsilon_{22,2}$  under the different loading conditions have also been presented in Fig. 10. As evident from Fig. 10, higher strain gradients are induced during compressive loading as compared to a shear load. Due to this, the maximum potential generated is on a higher side for the compressive load as compared to the shear load, as presented in Table 2. The strain gradients are directly linked to the potential generated due to the flexoelectric effect. Consequently, the potential difference under the compressive loading is higher in the region just beneath the centrosome (where microtubules are connected) owing to higher strain gradients as mentioned earlier in section 3.1.

### 3.3. Effect of variations of flexoelectric coefficients on the coupled electro-mechanical model

Due to the paucity of the experimental data related to flexoelectric coefficients for biomaterials in literature, the present study also evaluated the influence of flexoelectric coefficients ranging from  $1 \times 10^{-3}$ , 1 and  $1 \times 10^3$  nC/m that is adopted from the flexoelectric coefficients of isotropic inorganic compounds (Liu et al., 2012). Fig. 11 presents the effects of flexoelectric coefficients on the electric potential generated under the application of 60 nm compressive displacement at the top surface of the biological cell. As depicted in Fig. 11, the maximum value of the electric potential increases as the magnitude of the flexoelectric coefficient increases. The predicted values of the maximum electric potential from the coupled electro-mechanical model of the biological cell have been found to be 0.001 mV, 0.2 mV and 0.2 V for the flexoelectric coefficients of  $1 \times 10^{-3}$ , 1 and  $1 \times 10^3$  nC/m, respectively. Thus, the flexoelectric coefficient plays a significant role in the predicted electric potential and due consideration needs to be given in accounting the flexoelectric effect for accurately predicting the electro-elastic response, in particular at smaller length scales.

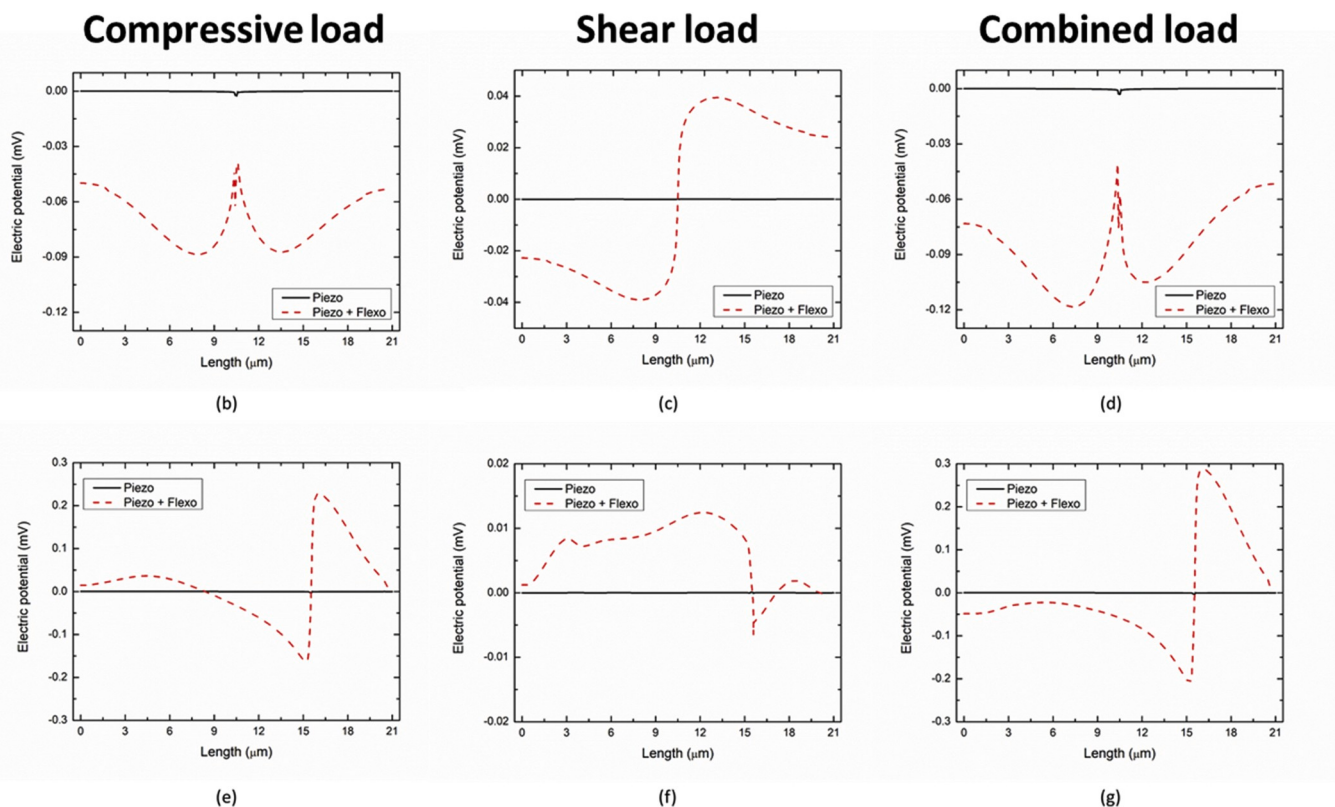
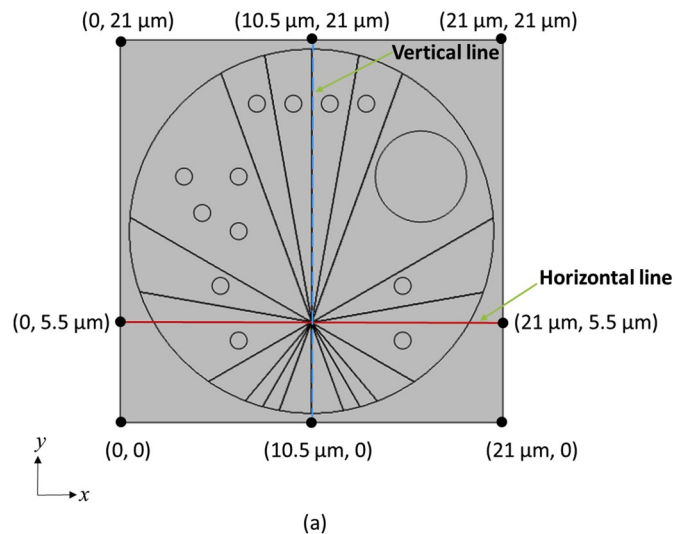


**Fig. 8.** (a) Schematic of two lines (horizontal and vertical) selected for comparing the outcomes of the coupled electro-mechanical model considering piezoelectric coupling alone and with both piezo and flexoelectric couplings. Comparative analysis of the electric potential (b-g) and electric field distribution (h-m) predicted across horizontal (b-d, h-j) and vertical (e-g, k-m) lines with and without consideration of flexoelectric coupling.

#### 3.4. Converse flexoelectric effect on a biological cell

The flexoelectric effect in biomaterials can be classified into two categories: the direct effect and the converse effect (Bruhn et al., 2016; Petrov, 2002; Wang et al., 2019; Chen et al., 2019; Jerusalem et al., 2019). The direct effect refers to the generation of electric potential under the application of mechanical force. While the converse effect is the reverse of direct effect and refers to the mechanical displacement induced within the material under the application of electric potential. The results mentioned in the aforementioned sections refer to the direct

effects. Notably, in cardiac cells and tissues, this direct effect is referred to as excitation-contraction coupling (ECC), an electro-mechanical process by which the electrical activation of cardiac myocytes results in an increase in the free intracellular calcium concentration that leads to the contraction of the heart muscle (Bers, 2001; Timmermann et al., 2017). Furthermore, there has also been extensive evidence about the reverse of ECC known as cardiac mechano-electric feedback (MEF), the mechanism by virtue of which the mechanical forces experienced by myocardial tissue alters their electrophysiological characteristics (Costabal et al., 2017; Franz and Bode, 2003; Prop et al., 2019; Quinn et al.,

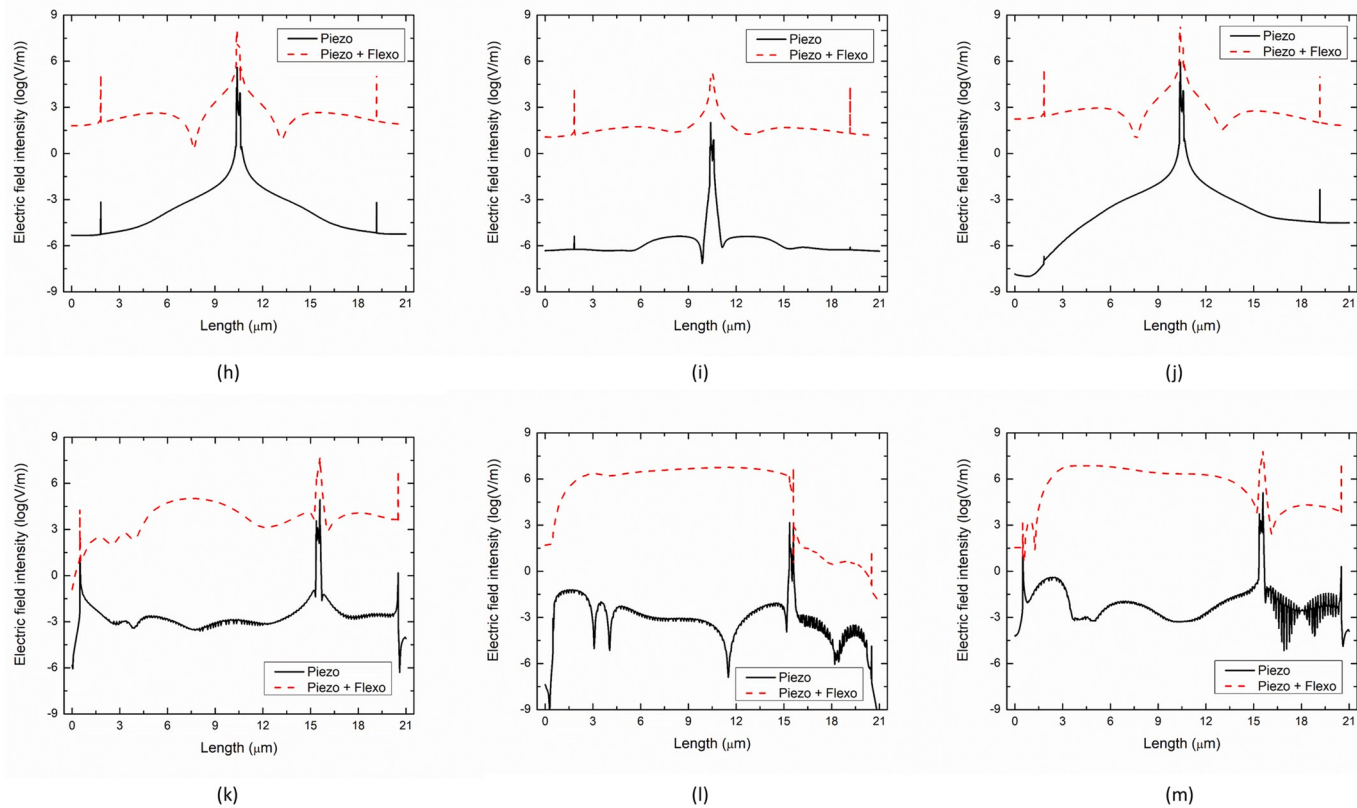


Fig. 8. (continued).

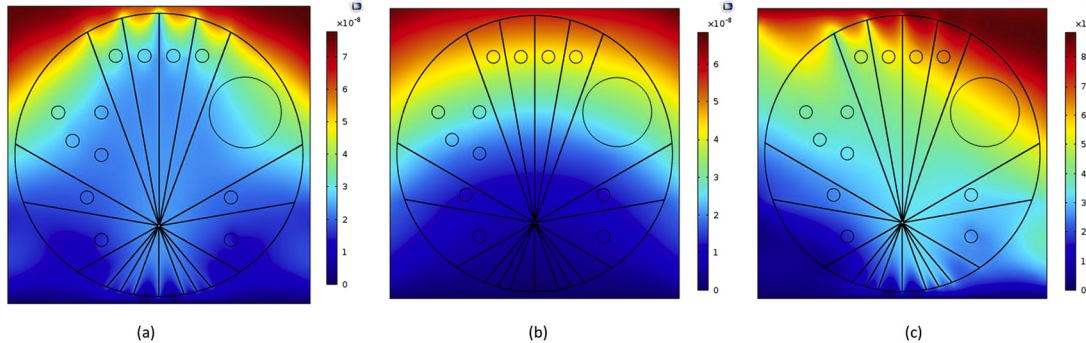


Fig. 9. The total displacement distribution (in m) within the biological cell with the application of 60 nm: (a) compressive load, (b) shear load, and (c) both compressive and shear loads at the top surface and with fixed bottom surface.

2014; Vikulova et al., 2016). The induction of mechanical effects on excitation has also been enumerated in isolated cells, cell membranes, multicellular preparations, and whole organs and organisms (Quinn et al., 2014; Vikulova et al., 2016). Thus, in this present study, simulations have also been conducted to quantify the converse effect, i.e. the mechanical response of the biological cell under the application of electric stimulation. In particular, a 100 mV electric potential (similar to (Bruhn et al., 2016)) has been applied at the top surface of the biological cell with a fixed and grounded bottom. The electro-elastic response of the converse flexoelectric effect has been shown in Fig. 12. In particular, the electric potential distribution within the biological cell has been presented in Fig. 12(a). While Fig. 12(b) presents the mechanical response of the biological cell under the application of electrical stimuli. The maximum displacement induced within the cell has been found to be close to 1 nm under the application of 100 mV electrical potential applied at the top surface. Further, as depicted in Fig. 12(b), the applied electrical stimuli at the top surface acts as a combined force with the

maximum magnitude of displacements induced on the top and right side of the biological cell. Fig. 12(c and d) presents the distribution of induced strain gradients  $\varepsilon_{11,1}$  and  $\varepsilon_{22,2}$ , respectively, under the application of electrical stimuli at the top surface. As evident from Fig. 12(c and d), higher strain gradients are mostly concentrated at the edges of the microtubule and cell membrane. This can be attributed to the fact that the microtubules (or cytoskeleton), which is the stiffest part of the biological cell that helps them to withstand both static and dynamic loads, are the first organelle to respond to any external stimuli and subsequently transmitting them to other organelles over both short and long timescales.

### 3.5. Effect of mechanical degradation of the cytoskeleton on the coupled electro-mechanical model

The cytoskeleton of the biological cell is dynamic during the entire lifecycle and can also be degraded resulting in considerable changes in

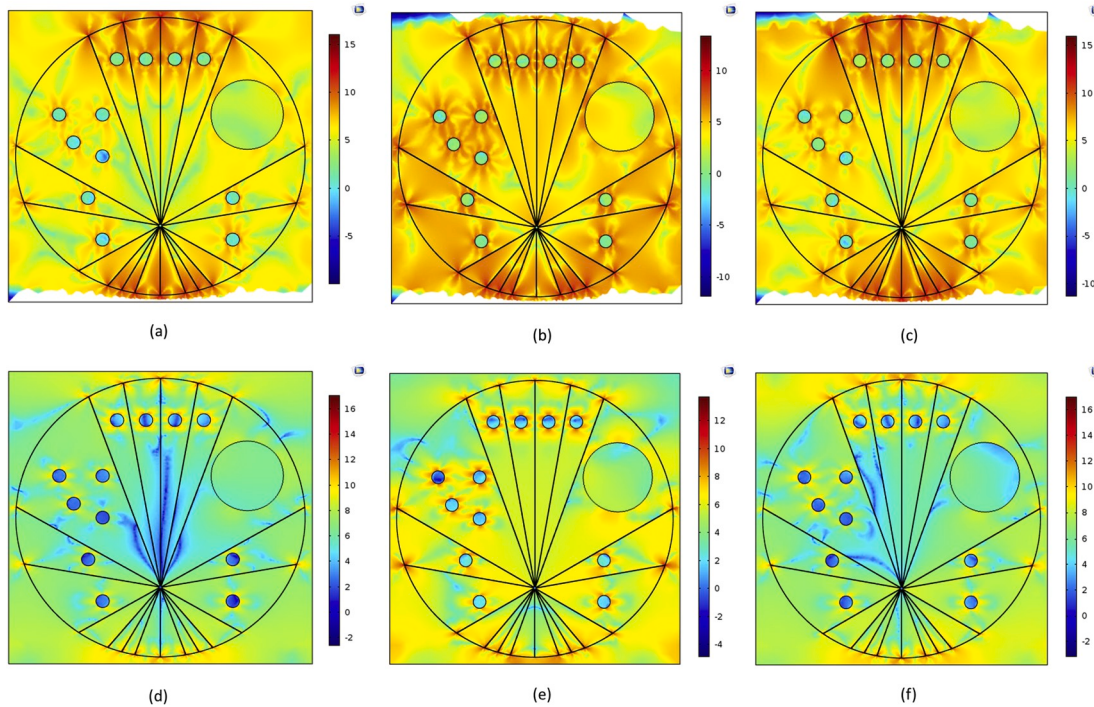


**Fig. 10.** The strain gradients (in logarithmic scale) induced within the biological cell with the application of 60 nm: (a, d) compressive load, (b, e) shear load and, (c, f) both compressive and shear loads. (a-c) represents  $\epsilon_{11,1}$  and (d-f) represents  $\epsilon_{22,2}$ .

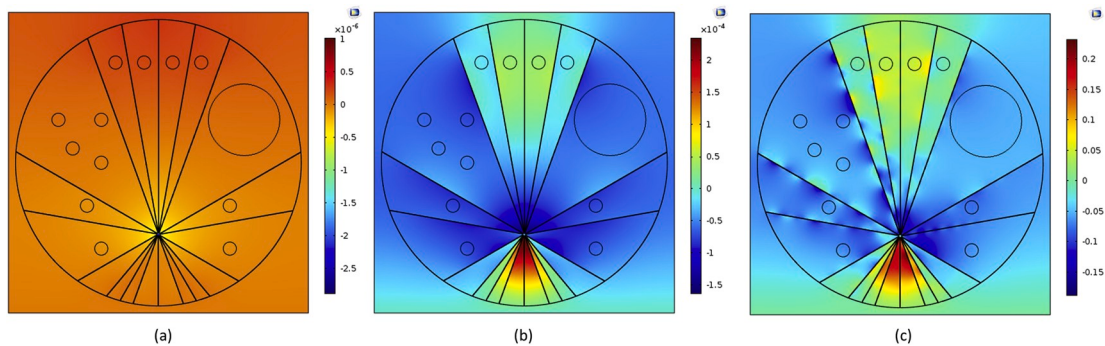


**Fig. 11.** Electric potential distribution (in V) predicted for different values of flexoelectric coupling coefficients: (a)  $1 \times 10^{-3}$  nC/m, (b) 1 nC/m, and (c)  $1 \times 10^3$  nC/m.

their elasticity owing to ageing or pathological diseases (Katti and Katti, 2017; Guz et al., 2014). Further, the cytoskeleton mechanics can also be disrupted due to the application of various anti-cancer drugs used for therapeutic treatment of cancerous cell. Moreover, *in vitro* studies reported in previous literature clearly indicates that the elastic modulus of cancerous cells is significantly lower as compared to the healthy cells (Abidine et al., 2018; Suresh, 2007a, 2007b). Thus, in the present study, the influence of degradation of the cytoskeleton has also been considered on the electro-elastic response of biological cells under external stimuli. The mechanical degradation of the cytoskeleton has been modelled by reducing the elastic moduli of the microtubules by 90 percent (Katti and Katti, 2017). The other structural features of the biological cells are maintained as it is. Fig. 13 presents the effects of the mechanically degraded cytoskeleton on the predicted piezoelectric and flexoelectric responses under the action of a 60 nm compressive load at the top surface of the biological cell. As depicted in Fig. 13, the degradation of microtubules by 90% results in a significant increase in the predicted piezoelectric voltage from 0.0005 mV to 0.002 mV. Further, flexoelectric coupling also results in a corresponding increase of electric potential from 0.2 mV to 0.25 mV for 90% degraded microtubules. This

can be attributed to the fact that the degraded microtubules will result in a larger magnitude of the deformation within the cytoplasm of the biological cell as compared to healthy microtubules and subsequently larger strain gradients.

### 3.6. Limitations and future directions

The present study models the biological cell as a two-dimensional composite comprising of different organelles having distinct material properties. A linearly coupled electro-mechanical model has been developed to quantify the cellular mechanics under the application of different magnitude and directions of external forces considering piezoelectric and nonlocal flexoelectric effects. However, number of limitations still prevail in this analysis. First and foremost is the basic assumption that the biological cell behaves as a linear elastic material, that has been actually derived from previous numerical modelling studies available in the literature (Katti and Katti, 2017; Garcia and Garcia, 2018a). In fact, the living cells are visco-elastic and the same has been elucidated by number experimental studies available in the literature, such as (Alcaraz et al., 2003; Efremov et al., 2017; Raman et al.,

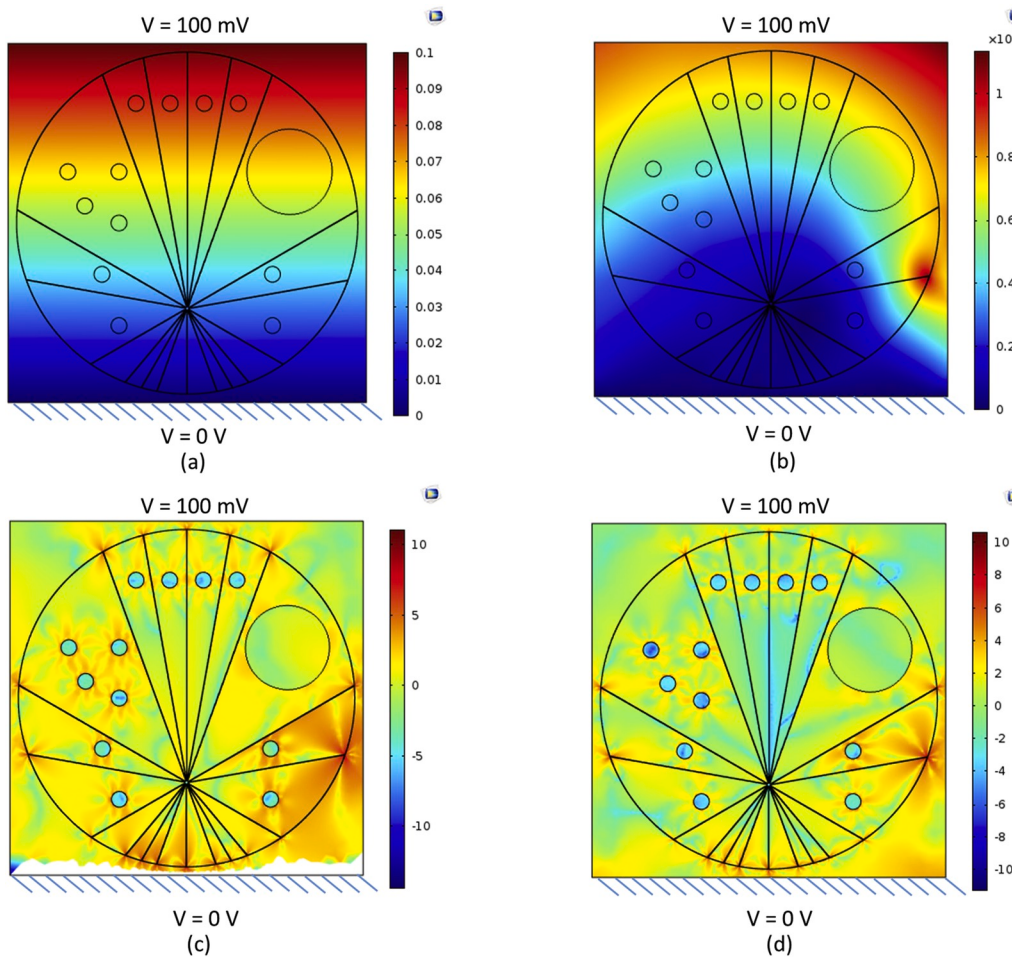


**Fig. 12.** Spatial distribution of: (a) electric potential (in V), (b) total displacement (in m), (c, d) strain gradients induced within the biological cell under the application of 100 mV electric potential applied at the top surface with a fixed and grounded bottom. (c) represents  $\epsilon_{11,1}$  and (d) represents  $\epsilon_{22,2}$ .

2011). Thus, it could be of great interest to quantify the electro-elastic response of biological cells considering the visco-elastic model presented in (Garcia and Garcia, 2018b; Pandolfi et al., 2017). Another major limitation of this study is the simplification of biological cells in the two-dimensional domain and the absence of dynamic response. Although, the present study was focused on developing the basic framework for capturing the electro-elastic response of the biological cell considering the most simplified model, incorporating the dynamic analysis in the three-dimensional model will definitely provide a more precise and accurate response of cellular mechanics and would assist in different promising avenues of medical technology ranging from sensing to energy harvesting devices fabrication. One of the possible extensions in the three-dimensional domain would be consideration of the cellular tensegrity model (McGarry and Prendergast, 2004; Ingber et al., 2014) whereby the individual components of the cytoskeleton, viz., microtubules, actin filaments and intermediate filaments are modelled using a discrete beam or truss elements. More recently a three-dimensional finite element bendo-tensegrity model of a eukaryotic cell has been reported in (Bansod et al., 2018) to quantify the mechanical response of cellular and sub-cellular components to external stimuli. Further, in the present analysis, the electro-elastic properties of the biological cells have been considered to be homogeneous and isotropic, addressing this issue could be one of the possible future extensions of the proposed model. Moreover, the electro-mechanical response of the biological cell can also be influenced by the inelastic mechanisms (damage and viscous effects) along with active responses, growth, remodeling, adhesion and migration (Ambrosi et al., 2019; Marino, 2019). Multiscale modelling

approaches could be utilized for capturing the nuances of such phenomena in the biological cells. The continuum formulation to model growth, differentiation and damage can be found in (Cyrus and Humphrey, 2014, 2017; Doblaré and García-Aznar, 2006) and the biophysical model to simulate cell adhesion and migration has been presented in (Vassaux et al., 2019). Thus, future studies are warranted for integrating such remarkable effects within the model and improve the accuracy of the proposed model. However, despite the aforementioned limitations, the developed coupled electro-mechanical model of a biological cell is one of the initial model that incorporates the piezoelectric and flexoelectric effects within the biological cell. The comparative analysis of the predicted outcomes of the model presented in this study would significantly assist in better understanding of the complex electro-mechanical response of the biological cell to external stimuli along with designing of electro-mechanical devices for different applications in the medical sciences.

#### 4. Conclusion

In this study, a computational model of the biological cell has been developed taking into account the electro-mechanical coupling of important physical effects such as linear piezoelectric and nonlocal flexoelectric effects. A two-dimensional model of the biological cell has been considered comprising of different key organelles that are subjected to different mechanical loading conditions from the extracellular side. It has been found that the effect of the inclusion of flexoelectric coupling in the electro-mechanical model is far more pronounced as

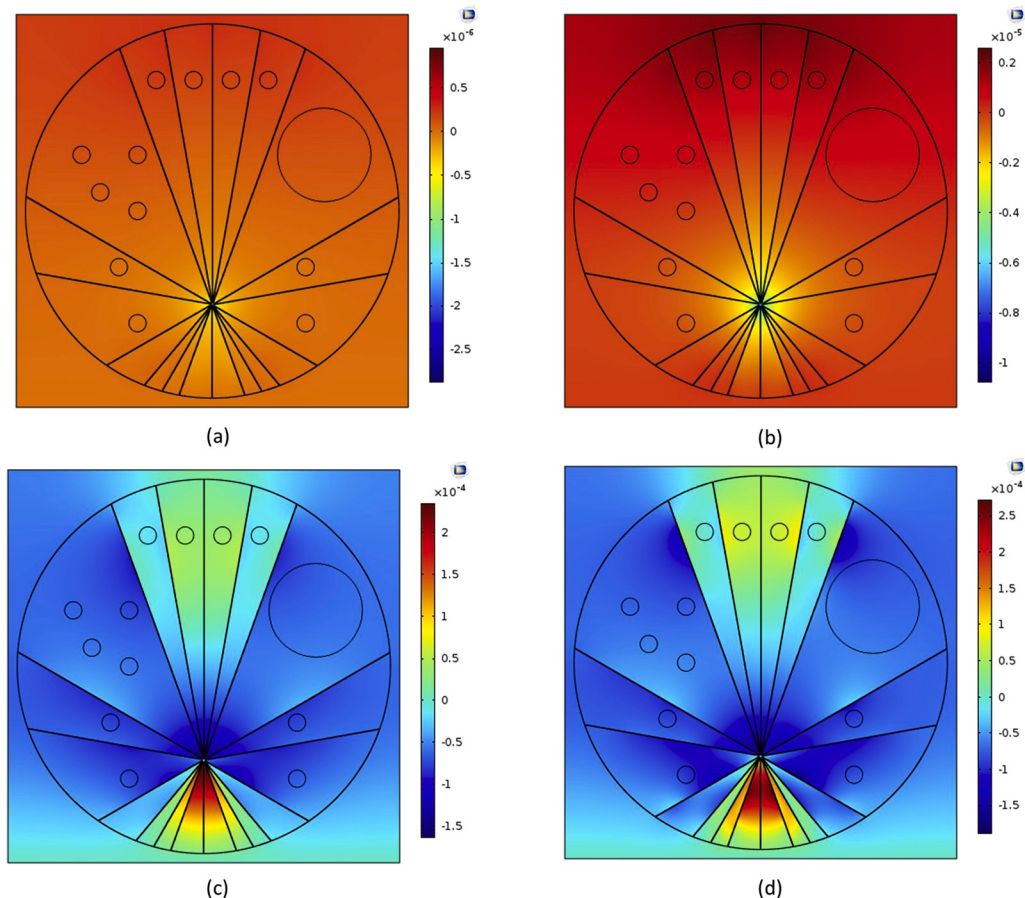


**Fig. 13.** Comparison of the electric potential distribution (in V) predicted with 60 nm compressive displacement at the top surface of biological cell for (a, c) 100% healthy cytoskeleton, and (b, d) mechanically degraded cytoskeleton by 90%. (a-b) is considering piezoelectric coupling while (c-d) is considering both piezo and flexoelectric couplings.

compared to including piezoelectric coupling alone. In its turn, this suggests that at smaller length scales the contribution of the flexoelectric coupling on the electro-mechanical response is quite significant and shall be accounted for accurately predicting the mechanics of biological cells under different loading conditions. It has been further revealed that the effect of compressive force on the biological cell results in enhanced electro-mechanical coupling in comparison to shear force. The results presented in the study further highlight that both the piezo and flexoelectric responses are dramatically affected by the mechanical degradation of the cytoskeleton. The developed model and the results presented in the study should be useful for our better understanding of the mechanics of biological cells that cannot be easily elucidated with experimental studies. The proposed model can be further extended for capturing the dynamics of the biological cells subjected to different boundary conditions using a three-dimensional domain and including additional cytoskeleton structures for extracting other useful and critical information of underlying mechanics at the cellular scale.

#### Author statement

**Sundeep Singh:** Methodology, Software, Formal analysis, Investigation, Data curation, Writing- Original draft preparation, Writing-Reviewing and Editing. **Jagdish A. Krishnaswamy:** Software, Writing-Reviewing and Editing. **Roderick Melnik:** Conceptualization, Supervision, Writing- Reviewing and Editing,

#### Acknowledgements

Authors are grateful to the NSERC and the CRC Program for their

support. RM is also acknowledging support of the BERC 2018-2021 program and Spanish Ministry of Science, Innovation and Universities through the Agencia Estatal de Investigacion (AEI) BCAM Severo Ochoa excellence accreditation SEV-2017-0718 and the Basque Government fund AI in BCAM EXP. 2019/00432. Authors are also grateful to Prof. Jack Tuszyński for useful discussions and providing a number of important references.

#### References

- Abdollahi, A., et al., 2014. Computational evaluation of the flexoelectric effect in dielectric solids. *J. Appl. Phys.* 116 (9), 093502.
- Abidine, Y., et al., 2018. Mechanosensitivity of cancer cells in contact with soft substrates using AFM. *Biophys. J.* 114 (5), 1165–1175.
- Ahmadpoor, F., Sharma, P., 2015. Flexoelectricity in two-dimensional crystalline and biological membranes. *Nanoscale* 7 (40), 16555–16570.
- Alcaraz, J., et al., 2003. Microrheology of human lung epithelial cells measured by atomic force microscopy. *Biophys. J.* 84 (3), 2071–2079.
- Ambrosi, D., et al., 2019. Growth and remodelling of living tissues: perspectives, challenges and opportunities. *J. R. Soc. Interface* 16 (157), 20190233.
- Anderson, J., Eriksson, C., 1970. Piezoelectric properties of dry and wet bone. *Nature* 227 (5257), 491–492.
- Bahrami-Samani, M., Patil, S.R., Melnik, R., 2010. Higher-order nonlinear electromechanical effects in wurtzite GaN/AlN quantum dots. *J. Phys. Condens. Matter* 22 (49), 495301.
- Bansod, Y.D., et al., 2018. A finite element bendo-tensegrity model of eukaryotic cell. *J. Biomech. Eng.* 140 (10).
- Barreto, S., et al., 2013. A multi-structural single cell model of force-induced interactions of cytoskeletal components. *Biomaterials* 34 (26), 6119–6126.
- Barvitenko, N., et al., 2018. Integration of intracellular signaling: biological analogues of wires, processors and memories organized by a centrosome 3D reference system. *Biosystems* 173, 191–206.
- Basoli, F., et al., 2018. Biomechanical characterization at the cell scale: present and prospects. *Front. Physiol.* 9, 1449.

- Bers, D., 2001. Excitation-contraction Coupling and Cardiac Contractile Force, vol. 237. Springer Science & Business Media.
- Bhowmik, A., Pilon, L., 2016. Can spherical eukaryotic microalgae cells be treated as optically homogeneous? *JOSA A* 33 (8), 1495–1503.
- Brown, J., Tuszyński, J., 1999. A review of the ferroelectric model of microtubules. *Ferroelectrics* 220 (1), 141–155.
- Bruhn, D.S., Lohmolt, M.A., Khandelia, H., 2016. Quantifying the relationship between curvature and electric potential in lipid bilayers. *J. Phys. Chem. B* 120 (21), 4812–4817.
- Chae, I., et al., 2018. Review on electromechanical coupling properties of biomaterials. *ACS Appl. Bio Mater.* 1 (4), 936–953.
- Chen, H., García-González, D., Jérusalem, A., 2019. Computational model of the mechanoelectrophysiological coupling in axons with application to neuromodulation. *Phys. Rev. E* 99 (3), 032406.
- Chen-Glasser, M., et al., 2018. Piezoelectric materials for medical applications. *Piezoelectricity—Organic and Inorganic Materials and Applications*. IntechOpen London, pp. 125–145.
- COMSOL Multiphysics v. 5.2, 2015. <https://www.comsol.com>.
- Costabal, F.S., et al., 2017. The importance of mechano-electrical feedback and inertia in cardiac electromechanics. *Comput. Methods Appl. Mech. Eng.* 320, 352–368.
- Cyron, C., Humphrey, J., 2014. Vascular homeostasis and the concept of mechanobiological stability. *Int. J. Eng. Sci.* 85, 203–223.
- Cyron, C., Humphrey, J., 2017. Growth and remodeling of load-bearing biological soft tissues. *Mecanica* 52 (3), 645–664.
- de Garcini, E.M., et al., 1990. Collagenous structures present in brain contain epitopes shared by collagen and microtubule-associated protein tau. *J. Struct. Biol.* 103 (1), 34–39.
- Dennig, D., et al., 2017. Piezoelectric tensor of collagen fibrils determined at the nanoscale. *ACS Biomater. Sci. Eng.* 3 (6), 929–935.
- Doblaré, M., García-Aznar, J., 2006. On numerical modelling of growth, differentiation and damage in structural living tissues. *Arch. Comput. Methods Eng.* 13 (4), 471.
- Efremov, Y.M., et al., 2017. Measuring nanoscale viscoelastic parameters of cells directly from AFM force-displacement curves. *Sci. Rep.* 7 (1), 1–14.
- Fallqvist, B., et al., 2016. Experimental and computational assessment of F-actin influence in regulating cellular stiffness and relaxation behaviour of fibroblasts. *J. Mech. Behav. Biomed. Mater.* 59, 168–184.
- Franz, M.R., Bode, F., 2003. Mechano-electrical feedback underlying arrhythmias: the atrial fibrillation case. *Prog. Biophys. Mol. Biol.* 82 (1–3), 163–174.
- Fukada, E., 1955. Piezoelectricity of wood. *J. Phys. Soc. Jpn.* 10 (2), 149–154.
- Fukada, E., 1968. Piezoelectricity as a fundamental property of wood. *Wood Sci. Technol.* 2 (4), 299–307.
- Fukada, E., 1983. Piezoelectric properties of biological polymers. *Q. Rev. Biophys.* 16 (1), 59–87.
- Fukada, E., 2000. History and recent progress in piezoelectric polymers. *IEEE Trans. Ultrason. Ferroelectrics Freq. Contr.* 47 (6), 1277–1290.
- Fukada, E., Yasuda, I., 1957. On the piezoelectric effect of bone. *J. Phys. Soc. Jpn.* 12 (10), 1158–1162.
- Fukada, E., Yasuda, I., 1964. Piezoelectric effects in collagen. *Jpn. J. Appl. Phys.* 3 (2), 117.
- Garcia, P.D., Garcia, R., 2018a. Determination of the elastic moduli of a single cell cultured on a rigid support by force microscopy. *Biophys. J.* 114 (12), 2923–2932.
- Garcia, P.D., Garcia, R., 2018b. Determination of the viscoelastic properties of a single cell cultured on a rigid support by force microscopy. *Nanoscale* 10 (42), 19799–19809.
- Gizzi, A., et al., 2015. Theoretical and numerical modeling of nonlinear electromechanics with applications to biological active media. *Commun. Comput. Phys.* 17 (1), 93–126.
- Gowrishankar, T.R., et al., 2006. Microdosimetry for conventional and supra-electroporation in cells with organelles. *Biochem. Biophys. Res. Commun.* 341 (4), 1266–1276.
- Guz, N., et al., 2014. If cell mechanics can be described by elastic modulus: study of different models and probes used in indentation experiments. *Biophys. J.* 107 (3), 564–575.
- Havelka, D., Cifra, M., 2009. Calculation of the electromagnetic field around a microtubule. *Acta Polytechnica* 49 (2).
- Havelka, D., et al., 2011. High-frequency electric field and radiation characteristics of cellular microtubule network. *J. Theor. Biol.* 286, 31–40.
- He, B., Javvaji, B., Zhuang, X., 2019. Characterizing flexoelectricity in composite material using the element-free galerkin method. *Energies* 12 (2), 271.
- Ingber, D.E., Wang, N., Stamenović, D., 2014. Tensegrity, cellular biophysics, and the mechanics of living systems. *Rep. Prog. Phys.* 77 (4), 046603.
- Jerusalem, A., et al., 2019. Electrophysiological-mechanical coupling in the neuronal membrane and its role in ultrasound neuromodulation and general anaesthesia. *Acta Biomater.* 97 (1), 116–140.
- Jiang, N., et al., 2017. Modeling the effects of lattice defects on microtubule breaking and healing. *Cytoskeleton* 74 (1), 3–17.
- Kalra, A., et al., 2019. On the Capacitive Properties of Individual Microtubules and their Meshworks arXiv preprint arXiv:1905.02865.
- Katti, D.R., Katti, K.S., 2017. Cancer cell mechanics with altered cytoskeletal behavior and substrate effects: a 3D finite element modeling study. *J. Mech. Behav. Biomed. Mater.* 76, 125–134.
- Kiran, R., et al., 2018. Poling direction driven large enhancement in piezoelectric performance. *Scripta Mater.* 151, 76–81.
- Kononova, O., et al., 2014. Tubulin bond energies and microtubule biomechanics determined from nanoindentation in silico. *J. Am. Chem. Soc.* 136 (49), 17036–17045.
- Krishnaswamy, J.A., et al., 2019a. Design of lead-free PVDF/CNT/BaTiO<sub>3</sub> piezocomposites for sensing and energy harvesting: the role of polycrystallinity, nanoadditives, and anisotropy. *Smart Mater. Struct.* 29 (1), 15021.
- Krishnaswamy, J.A., et al., 2019b. Lead-free piezocomposites with CNT-modified matrices: accounting for agglomerations and molecular defects. *Compos. Struct.* 224, 111033.
- Krishnaswamy, J.A., et al., 2019c. Improving the performance of lead-free piezoelectric composites by using polycrystalline inclusions and tuning the dielectric matrix environment. *Smart Mater. Struct.* 28 (7), 75032.
- Krishnaswamy, J.A., et al., 2020. Advanced modeling of lead-free piezocomposites: the role of nonlocal and nonlinear effects. *Compos. Struct.* 238 (15), 111967.
- Kučera, O., Havelka, D., 2012. Mechano-electrical vibrations of microtubules—link to subcellular morphology. *Biosystems* 109 (3), 346–355.
- Kushagra, A., 2015. Thermal fluctuation induced piezoelectric effect in cytoskeletal microtubules: model for energy harvesting and their intracellular communication. *J. Biomed. Sci. Eng.* 8, 511 (08).
- Labanca, M., et al., 2008. Piezoelectric surgery: twenty years of use. *Br. J. Oral Maxillofac. Surg.* 46 (4), 265–269.
- Li, Y., et al., 2015. Analysis of mitochondrial mechanical dynamics using a confocal fluorescence microscope with a bent optical fibre. *J. Microsc.* 260 (2), 140–151.
- Li, S., Wang, C., Nithiarasu, P., 2017. Three-dimensional transverse vibration of microtubules. *J. Appl. Phys.* 121 (23), 234301.
- Li, M., et al., 2018. Nanoscale characterization of dynamic cellular viscoelasticity by atomic force microscopy with varying measurement parameters. *J. Mech. Behav. Biomed. Mater.* 82, 193–201.
- Liew, K., Xiang, P., Zhang, L., 2015. Mechanical properties and characteristics of microtubules: a review. *Compos. Struct.* 123, 98–108.
- Liu, C., Hu, S., Shen, S., 2012. Effect of flexoelectricity on electrostatic potential in a bent piezoelectric nanowire. *Smart Mater. Struct.* 21 (11), 115024.
- Madden, J.D., et al., 2004. Artificial muscle technology: physical principles and naval prospects. *IEEE J. Ocean. Eng.* 29 (3), 706–728.
- Mao, S., Purohit, P.K., 2014. Insights into flexoelectric solids from strain-gradient elasticity. *J. Appl. Mech.* 81 (8), 081004.
- Marcotti, S., Reilly, G.C., Lacroix, D., 2019. Effect of cell sample size in atomic force microscopy nanoindentation. *J. Mech. Behav. Biomed. Mater.* 94, 259–266.
- Marino, M., 2019. Constitutive Modeling of Soft Tissues.
- McGarry, J., Prendergast, P., 2004. A three-dimensional finite element model of an adherent eukaryotic cell. *Eur. Cell. Mater.* 7, 27–33.
- Melnik, R.V., Wei, X., Moreno-Hagelsieb, G., 2009. Nonlinear dynamics of cell cycles with stochastic mathematical models. *J. Biol. Syst.* 17, 425–460 (03).
- Newnham, R.E., 2005. *Properties of Materials: Anisotropy, Symmetry, Structure*. Oxford University Press.
- Nguyen, T.D., et al., 2013. Nanoscale flexoelectricity. *Adv. Mater.* 25 (7), 946–974.
- Ofek, G., Wiltz, D.C., Athanasiou, K.A., 2009. Contribution of the cytoskeleton to the compressive properties and recovery behavior of single cells. *Biophys. J.* 97 (7), 1873–1882.
- Pandolfi, A., Gizzi, A., Vasta, M., 2016. Coupled electro-mechanical models of fiber-distributed active tissues. *J. Biomech.* 49 (12), 2436–2444.
- Pandolfi, A., Gizzi, A., Vasta, M., 2017. Visco-electro-elastic models of fiber-distributed active tissues. *Mecanica* 52 (14), 3399–3415.
- Parton, V.Z., Kudryavtsev, B.A., 1988. *Electromagnetoelasticity: Piezoelectrics and Electrically Conductive Solids*. Taylor & Francis.
- Petrov, A.G., 2002. Flexoelectricity of model and living membranes. *Biochim. Biophys. Acta Biomembr.* 1561 (1), 1–25.
- Propst, A., et al., 2019. An orthotropic electro-viscoelastic model for the heart with stress-assisted diffusion. *Biomech. Model. Mechanobiol.* 1–27.
- Quinn, T.A., Kohl, P., Ravens, U., 2014. Cardiac mechano-electric coupling research: fifty years of progress and scientific innovation. *Prog. Biophys. Mol. Biol.* 115 (2–3), 71–75.
- Raman, A., et al., 2011. Mapping nanomechanical properties of live cells using multi-harmonic atomic force microscopy. *Nat. Nanotechnol.* 6 (12), 809.
- Saputra, A.A., et al., 2018. Micromechanics determination of effective material coefficients of cement-based piezoelectric ceramic composites. *J. Intell. Mater. Syst. Struct.* 29 (5), 845–862.
- Setayandeh, S., Lohrasebi, A., 2016. Multi scale modeling of 2450 MHz electric field effects on microtubule mechanical properties. *J. Mol. Graph. Model.* 70, 122–128.
- Shamos, M.H., Lavine, L.S., 1967. Piezoelectricity as a fundamental property of biological tissues. *Nature* 213 (5073), 267.
- Sharma, N., Landis, C.M., Sharma, P., 2010. Piezoelectric thin-film superlattices without using piezoelectric materials. *J. Appl. Phys.* 108 (2), 024304.
- Suresh, S., 2007a. Biomechanics and biophysics of cancer cells. *Acta Biomater.* 3 (4), 413–438.
- Suresh, S., 2007b. Nanomedicine: elastic clues in cancer detection. *Nat. Nanotechnol.* 2 (12), 748.
- Thackston, K.A., Deheyn, D.D., Sievenpiper, D.F., 2019. Simulation of electric fields generated from microtubule vibrations. *Phys. Rev. 100* (2), 022410.
- Timmermann, V., et al., 2017. An integrative appraisal of mechano-electric feedback mechanisms in the heart. *Prog. Biophys. Mol. Biol.* 130, 404–417.
- Tiwari, P.K., et al., 2009. Modeling of nanoparticle-mediated electric field enhancement inside biological cells exposed to AC electric fields. *Jpn. J. Appl. Phys.* 48 (8R), 087001.
- Uchino, K., 2009. *Ferroelectric Devices*. CRC press.
- Vassaux, M., et al., 2019. A biophysical model for curvature-guided cell migration. *Biophys. J.* 117 (6), 1136–1144.
- Vikulova, N.A., et al., 2016. Mechano-electric feedback in one-dimensional model of myocardium. *J. Math. Biol.* 73 (2), 335–366.

- Wang, X., et al., 2010. Electricity generation based on one-dimensional group-III nitride nanomaterials. *Adv. Mater.* 22 (19), 2155–2158.
- Wang, B., et al., 2019. Flexoelectricity in solids: progress, challenges, and perspectives. *Prog. Mater. Sci.* 106, 100570.
- Xiang, P., Liew, K.M., 2012. Dynamic behaviors of long and curved microtubules based on an atomistic-continuum model. *Comput. Methods Appl. Mech. Eng.* 223, 123–132.
- Xue, F., et al., 2015. Effect of membrane stiffness and cytoskeletal element density on mechanical stimuli within cells: an analysis of the consequences of ageing in cells. *Comput. Methods Biomech. Biomed. Eng.* 18 (5), 468–476.